REPORT DOCUMENTATION PAGE

Form Approved
OMB No. 0704-0188

PLEASE DO NOT RETURN YOUR FORM TO THE ABOVE ORGANIZATION.

1. REPORT DATE *(DD-MM-YYYY)*	2. REPORT TYPE	3. DATES COVERED *(From - To)*
27-03-2006	Final	Mar-Dec 2005

4. TITLE AND SUBTITLE
Advanced Neural Network Modeling of Synthetic Jet Flow Fields

5a. CONTRACT NUMBER

5b. GRANT NUMBER
FA9550-05-1-0175

5c. PROGRAM ELEMENT NUMBER

6. AUTHOR(S)
Orkwis, Paul D.
Daviaux, Terry

5d. PROJECT NUMBER

5e. TASK NUMBER

5f. WORK UNIT NUMBER

7. PERFORMING ORGANIZATION NAME(S) AND ADDRESS(ES)
University of Cincinnati
Dept. AsE&EM, ML 70
Cincinnati, OH 45221-0070

8. PERFORMING ORGANIZATION REPORT NUMBER

9. SPONSORING/MONITORING AGENCY NAME(S) AND ADDRESS(ES)
U.S. Air Force Office of Scientific Research
4015 Wilson Blvd. Rm. 713
Arlington, VA 22203

10. SPONSOR/MONITOR'S ACRONYM(S)
AFOSR/NA

11. SPONSOR/MONITOR'S REPORT NUMBER(S)

12. DISTRIBUTION/AVAILABILITY STATEMENT
Approved for public release,
distribution unlimited

AFRL-SR-AR-TR-07-0469

13. SUPPLEMENTARY NOTES

14. ABSTRACT

The purpose of this research was to continue development of a neural network-based, lumped deterministic source term (LDST) approximation module for modeling synthetic jets in large-scale CFD calculations. The LDST approximation technique developed by the author and his students was employed. The main exploration involved the grid sensitivity of the neural network model. A second task was originally planned on the portability of the approach to other solvers, but interesting developments on the first task prevented that study from being pursued.

15. SUBJECT TERMS
Synthetic jets, deterministic source terms, lumped deterministic source terms, neural network modeling, lower order modeling, computational fluid dynamics

16. SECURITY CLASSIFICATION OF:			17. LIMITATION OF ABSTRACT	18. NUMBER OF PAGES	19a. NAME OF RESPONSIBLE PERSON
a. REPORT	b. ABSTRACT	c. THIS PAGE			Professor Paul D. Orkwis
U	U	U	UU	17	19b. TELEPHONE NUMBER *(Include area code)* 1-513-556-3366

ADVANCED NEURAL NETWORK MODELING OF SYNTHETIC JET FLOW FIELDS

AFOSR GRANT NUMBER FA9550-05-1-0175

Final Report

Paul D. Orkwis
Department of Aerospace Engineering
University of Cincinnati

Abstract

The purpose of this research was to continue development of a neural network-based, lumped deterministic source term (LDST) approximation module for modeling synthetic jets in large-scale CFD calculations. The LDST approximation technique developed by the author and his students was employed. The main exploration involved the grid sensitivity of the neural network model. A second task was originally planned on the portability of the approach to other solvers, but interesting developments on the first task prevented that study from being pursued.

Objectives

The original goals of the proposed research effort were to:

1. Demonstrate the Grid Insensitivity of the Neural Network-Lumped Deterministic Source Terms for Synthetic Jets.
2. Show that the approach is portable to other solvers.

Details of the first objective only will be presented since the actual research work focused on this aspect after initial studies found it to be most promising.

The synthetic jet neural network lumped deterministic source term model developed under previous AFOSR support assumed the use of identical main-flow grids for both the training data and the eventual application. This was done as an initial step toward demonstrating the feasibility of the approach with the intention of creating a more general model later by retraining the neural network with cell volume as a parameter, thereby putting the LDSTs on a per unit volume basis. The major modification to the approach was to then retrain the neural network with existing data and including cell volume with cell location as inputs. The worked progressed as described below:

1. Previously computed synthetic jet cases were gathered including their resultant LDSTs.
2. A procedure was developed to utilize the original LDST on general grids using a transfer function.
3. The neural network performance was compared on a new grid against that on the original training grid to assess the accuracy of the modified approach.
4. Tthe accuracy of the resultant model was then assessed via a coarsened grid in the axial direction.

5. The relationship between main-flow axial grid spacing and model accuracy was determined.
6. The minimum axial grid resolution requirements for effective NN-LDST modeling was determined.

Two additional approaches were proposed to obtain a grid independent NN-LDST approach. The following sections describe the LDST approach in general, the Neural Network interpolation procedure, the Numerical Procedure and then Results obtained and reported in AIAA Paper 2006-0321.

LDST Approach

The following paragraphs describe the lumped deterministic source term concept. This presentation uses the inviscid form of the 2*D* governing equations for clarity, specifically the mass, x and y momentum, and energy equation. Viscous terms and the third dimension are included in the actual equations used in this work.

The Lumped Deterministic Source Term methodology can be described from the continuous governing equations, Eq. 1, but is applied to their discrete form.

$$\frac{\partial \rho}{\partial t}+\frac{\partial}{\partial x}(\rho u)+\frac{\partial}{\partial y}(\rho v)=0$$

$$\frac{\partial}{\partial t}(\rho u)+\frac{\partial}{\partial x}(\rho u^2+p)+\frac{\partial}{\partial y}(\rho uv)=0 \qquad (1)$$

$$\frac{\partial}{\partial t}(\rho v)+\frac{\partial}{\partial x}(\rho uv)+\frac{\partial}{\partial y}(\rho v^2+p)=0$$

$$\frac{\partial(\rho e_t)}{\partial t}+\frac{\partial}{\partial x}[(\rho e_t+p)u]+\frac{\partial}{\partial y}[(\rho e_t+p)v]=0$$

When the time derivatives are zero, the spatial derivatives represent the steady state governing equations. For numerical simulations these terms are often called the solution residual, $R_k(Q)$ (here $k=1,...,4$), as illustrated below:

$$R_1(Q)=\frac{\partial}{\partial x}(\rho u)+\frac{\partial}{\partial y}(\rho v)=0$$

$$R_2(Q)=\frac{\partial}{\partial x}(\rho u^2+p)+\frac{\partial}{\partial y}(\rho uv)=0$$

$$R_3(Q) = \frac{\partial}{\partial x}(\rho uv) + \frac{\partial}{\partial y}(\rho v^2 + p) = 0 \tag{2}$$

$$R_4(Q) = \frac{\partial}{\partial x}[(\rho e_t + p)u] + \frac{\partial}{\partial y}[(\rho e_t + p)v] = 0$$

$$Q = [\rho, \rho u, \rho v, \rho e_t]^T$$

It is important to note that the conserved variable vector Q, which satisfies equation (2), is not the same as $\overline{Q}$, the time-average of an unsteady solution. This difference can be observed and the LDST's defined by considering the vector residual operator, $R_k(Q)$.

To better understand this, start by considering the conservative variable vector Q for an unsteady flow, which can be represented as:

$$Q = \overline{Q} + \tilde{Q} + Q' \tag{3}$$

where $\overline{Q}$ is the time-averaged value of Q over a large time ΔT (to be distinguished from the short-time Favre-averaged value), $\tilde{Q}$ is a deterministic unsteady fluctuation and Q' is the stochastic fluctuation.

The decomposed conservative variables are then substituted into the unsteady governing equations and the stochastic terms ignored for the sake of clarity in this discussion (the stochastic terms are modeled in the usual manner via approximations of the Reynolds stress terms). Since these equations are nonlinear, the resulting equation set consists of three distinct sets of terms: terms containing only $\overline{Q}$ products, terms containing only $\tilde{Q}$ products and terms containing a mixture of $\overline{Q}$ and $\tilde{Q}$ variables. Similar to the Favre decomposition, upon time averaging all the linear $\tilde{Q}$ terms, the unsteady terms vanish so that one is left with the steady state residual operator acting on the time-averaged solution plus the time average of all the higher order perturbation terms. It is the higher order perturbation terms that define the effect of unsteadiness in the steady state solution. The LDST's can be obtained from the time averaged solution as:

$$R_k(\overline{Q}) + \mathrm{LDST}_k = 0. \tag{4}$$

Again, note that the first term in Eq (4) is the usual residual operator $R_k(Q)$, while the second term represents the source terms that must be added to the steady state equations to include the effect of unsteadiness, i.e., the lumped deterministic source terms. The two solutions, one obtained from the steady state equation ($R_k(Q) = 0$) and the solution of Eq (4) are different, since the second represents the time average of an unsteady solution and includes the effect of unsteadiness on the flow, while the first does not.

Interestingly, the continuity equation, since it is linear in the conservative variables, reduces upon variable decomposition and time averaging to:

$$\frac{\partial}{\partial x}(\overline{\rho u}) + \frac{\partial}{\partial y}(\overline{\rho v}) = 0 \tag{5}$$

This implies that the mass source terms should be identically zero, assuming that there is no mass generation:

$$\mathrm{LDST}_1 = R_1\left(\overline{Q}\right) = 0. \tag{6}$$

For completeness, it should be noted that for viscous flows the source terms are again equal to the negative of the steady state residual and found in a similar manner. This also includes the turbulence model equations, in this case ρk and $\rho\varepsilon$.

To summarize, the lumped deterministic source terms are found by forming the time mean of the unsteady conservative variable vector and applying the residual operator to it. Using this technique, the unsteady effects and the influence of small geometric details can be included in simulations that do not compute these structures. However, a means to predict the source terms is needed to avoid repeated computation of the unsteady solution. Neural networks can be used for this purpose if the source terms are reasonable functions of some governing parameters. The next section describes the procedure used to develop the neural network-based source terms for flows of this type.

Neural Network

In the current work a neural network was used to obtain the LDST's. This NN was based on the fast and accurate Levenberg-Marquard back propagation algorithm[21,22]. A neural network is a system that, thanks to its topological structure, can adaptively learn nonlinear mappings from input to output space when the network has a large database of prior examples from which to learn. It simulates human functions such as learning from experience, generalizing from previous to new data, and abstracting essential characteristics from inputs containing irrelevant data.

The basic architecture of a neural network consists of layers of interconnected processing units – called neurons (comparable to the dendrites in the biological neuron), which transform an input vector $[p_1, p_2, ..., p_M]$ into an output vector $[a_1, a_2, ..., a_S]$. Neurons without predecessors are called input neurons and constitute the input layer. All the other neurons are called computational units. A nonempty subset of the computational units is specified as the output units. All the computational units that are not output neurons are called hidden neurons. Each interconnection between two neurons $n_i \rightarrow n_j$ has an associated weight factor w_{ij} and bias b_i that can be adjusted by using an appropriate learning algorithm like the Levenberg-Marquardt[21,22] method. The network used in this work will have the number of neurons in the hidden layer which will minimize the mean square error.

Neural networks are used for modeling complex data relationships. The Universal Approximation Theorem[23,24,25] says that a neural network with one hidden layer is able to approximate any continuous function f: $R^M \rightarrow R^S$ (M, S are dimensions of the function domain and range, respectively) in any domain with a given accuracy. Features of the input data are extracted in the hidden layer with a hyperbolic tangent transfer function, and in the output layer with a pure linear transfer function. Based on the theorem and due to the topological structure of the neural network one can generate complex data dependencies without performing time-consuming computations.

In this work, the neural network was trained to generate source terms for any combination of input parameters $\{x, y, M\}$, where M is the initial Mach number of the cross flow. The source terms on a unit volume basis were then used to include the effect of the SJ unsteadiness in steady state calculations of flow fields without the presence of a cavity. Every case computed with

unsteady computations produces five source terms for each grid cell, corresponding to the 2 momentum equation components, the energy equation and the k and ϵ turbulence model equations. In other words, the five source terms are functions of the initial Mach number and of the local x and y coordinates. The data consisting of each individual source term at all of the x and y coordinates for all the test cases were stored in a series of vectors. Two cases were eliminated in order to see how the neural network could reproduce the source terms once the network had been trained. The vectors were then randomly reordered to achieve efficient training and then divided into training data (75 %) and testing data (25 %). The latter are used to determine the error when the network generates data it has never seen before. This error is used to set a stopping criterion, so that the network does not "over fit" data by continued training after the testing error has reached its minimum. The training process is then stopped and the weights corresponding to the minimum testing error are used to generate the source terms. In this work the neural network generates source terms that are then used to run steady computations. Consequently the method is interesting for large-scale simulations in which it is difficult to include the influence of devices like SJs because of their dimensions. The next section states the details of the numerical technique used in this research.

Numerical Procedure

The commercial CFD package CFD++ from Metacomp Technologies was used for the simulations. A multi-dimensional higher-order Total Variation Diminishing interpolation was used to avoid spurious numerical oscillations in the computed flow fields[26]. These polynomials are exact fits of multi-dimensional linear data. An approximate Riemann solver was used to define upwind fluxes and preconditioning used for low-speed flows. The code as employed in this study has second-order spatial accuracy, fourth-order accuracy in time, and a finite-volume framework. A wall-distance-free cubic k-ϵ turbulence model[27] was adopted. This model is tensorially invariant and frame-indifferent. It accounts for normal-stress anisotropy, swirl and streamline curvature effects.

Boundary and Initial Conditions

Unsteady Computations

For these simulations the boundary conditions were total temperature, k and ϵ on the inflow plane and back-pressure on the upper and outflow planes. All the solid surfaces were imposed with no-slip adiabatic wall conditions while the piston was set as an oscillating no-slip adiabatic wall. The amplitude(A) and frequency(f) of the piston were imposed using the normal-component of the wall velocity

$$v_n = A\sin(\omega t) \tag{7}$$

where the angular velocity, $\omega = 2\pi f$. The initial conditions imposed everywhere were total pressure, density and u-velocity.

Previous studies[19], performed in an effort to explore the variation of the synthetic jet performance with frequency and amplitude of the plenum oscillation, suggested that a synthetic jet operates best at the Helmholtz frequency. The results of the current research were obtained with that frequency.

Steady Computations

Again total temperature, k and ϵ were imposed on the inflow plane and backpressure on the upper and outflow planes. Velocities at the exit of the orifice were extracted from the time-averaged unsteady simulations; these velocities were then used as inflow/outflow conditions at the orifice interface. The flow variable values were then frozen at this interface. This assured the correct velocities were obtained at the interface even when the jet was not physically present in the simulation.

Grids

A structured and an unstructured mesh were created for this study: the cavity and orifice were omitted from each of the meshes for the steady computations. The number of grid points was selected to achieve the condition $y^+ < 1$ for the first cell off the wall in all cases. This condition permitted the computation of boundary layers on all the surfaces for different SJ operating conditions. The commercial grid generation software package, Gambit, was used to create the computational meshes. The Cartesian coordinate system was chosen oriented with its origin at the centerline of the orifice exit. The dimensions of the cavity were $[32.0mm \times 12.25mm]$, while the width of the orifice was $h = 1.0mm$. The ratio of orifice diameter to cavity diameter was $d_o / d_c = 1/32$. Figure 1 illustrates the structured mesh and Figure 2 displays the unstructured mesh. Figure 3 shows a contour plot of the cell area for each of the grids, verifying the change in grid density.

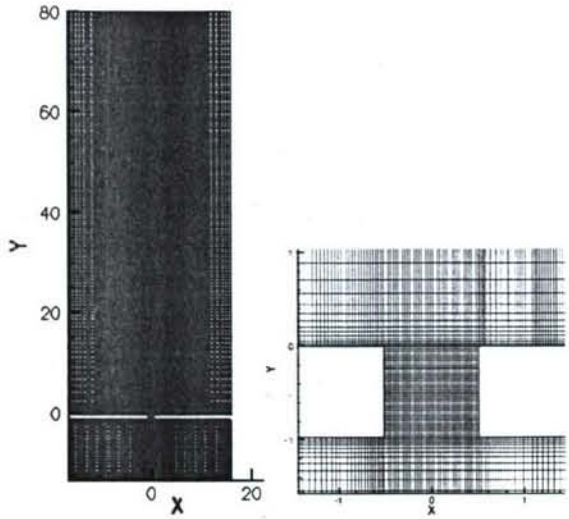

Figure 1. Structured Mesh with Enlarged Orifice

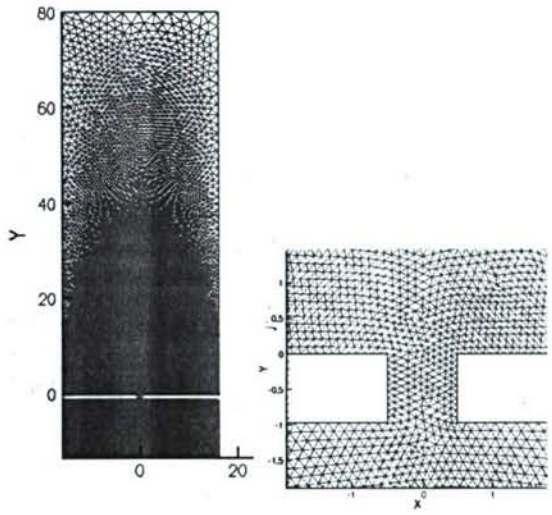

Figure 2. Unstructured Mesh with Enlarged Orifice

Cyclic Convergence

The pressure in one cell at the middle of the plenum back wall was probed to determine when the solution reached a cyclic state. The code was run for approximately 30 characteristic times of this signal to allow the solutions to become periodic, which for many cases took tens of

thousands of iterations. In the case of time-average simulations with source terms inserted in the governing equations, two thousand iterations were sufficient to achieve convergence.

Analysis

A commercial software visualization package, Tecplot, was used to visualize the results. Successive images over the period of a cycle were animated for the unsteady data visualization: pressure and vorticity contours were used. Contour plots of the LDST's were also plotted and compared for each of the grids. The authors also computed the momentum thickness at 10 *mm* downstream of the orifice centerline using the equation:

$$\theta = \int_0^{y_1} \frac{\rho u}{\rho_e u_e} \cdot \left(1 - \frac{u}{u_e}\right) dy, \tag{8}$$

Where ρ_e and u_e are the density and x-velocity evaluated at $y = y_1$ which corresponds to free stream conditions. Both instantaneous and average momentum thickness were computed. The next section concerns the results obtained with this approach.

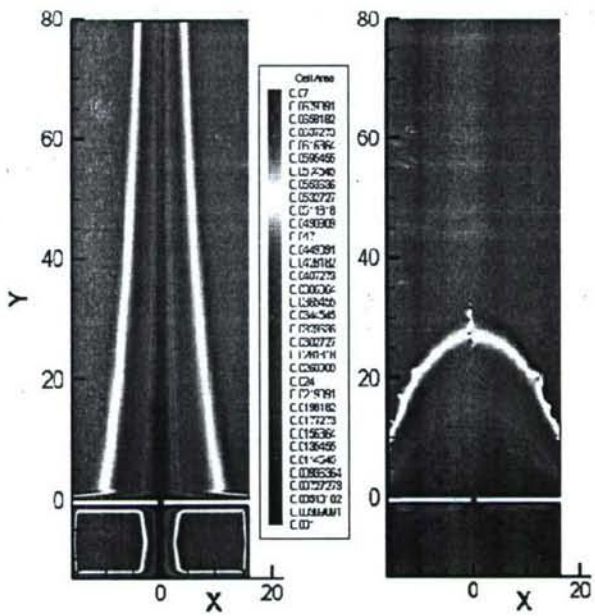

Figure 3. (Left), Cell Volume for Structured Mesh (Right), Cell Volume for Unstructured Mesh

Results

The focus of this work was to explore the grid dependence of the NN-LDST approach. The work extends results obtained in a previous work where the initial Mach number of the flow was varied.[18] The Mach number ranges from 0.15 to 0.6 in increments of 0.05. Both structured and unstructured meshes were used to compute the unsteady and time averaged solutions to demonstrate their equivalence. The LDSTs from both cases are then compared in their basic form and on a per cell area basis to demonstrate that the latter is universal. They are then applied in a steady solver to recreate the time average solution and demonstrate that both approaches lead to similar results. The NN-LDST's from the original structured mesh are then applied to coarsened meshes in order to determine the grid coarseness limits of the approach and to show that the NN-LDST approach can be used on general meshes.

Structured and Unstructured Meshes

Figures 4 and 5 show contours of the energy, x-momentum, and the y-momentum on the structured (Left) and unstructured (Right) meshes for the case when the Mach number equals 0.15. It is apparent from the figures that while the results are similar in many respects they are very different and beg the question as to whether or not the approach can be applied in a general way or if a separate neural network needs to be trained for each grid. Clearly this would be unacceptable.

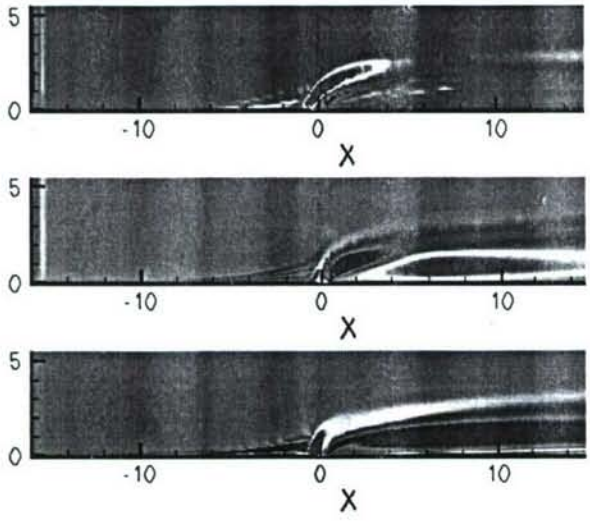

Figure 4 M=0.15, (Top)Structured Mesh Energy Source Term, (Center)Structured Mesh X-Momentum Source Term, (Bottom)Structured Mesh Y-Momentum Source Term

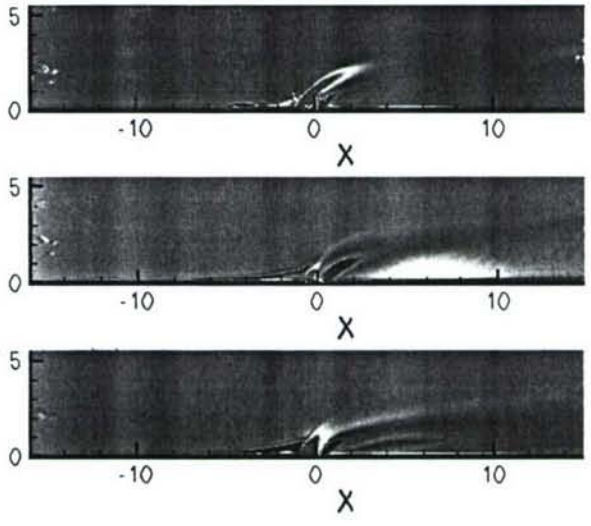

Figure 5 M=0.15, (Top)Unstructured Mesh Energy Source Term, (Center)Unstructured Mesh X-Momentum Source Term, (Bottom)Unstructured Mesh Y-

Figure 6 shows the same source terms divided by their cell areas. It is important to note that although the solutions are still slightly different the LDSTs on a per cell area basis are clearly comparable. This leads one to conclude that the NN-LDST approach can be applied to different grids if either trained with cell area as a parameter or if trained on a specific grid and interpolated

to another using the per cell area values. The latter approach is taken in this work to demonstrate that it is possible.

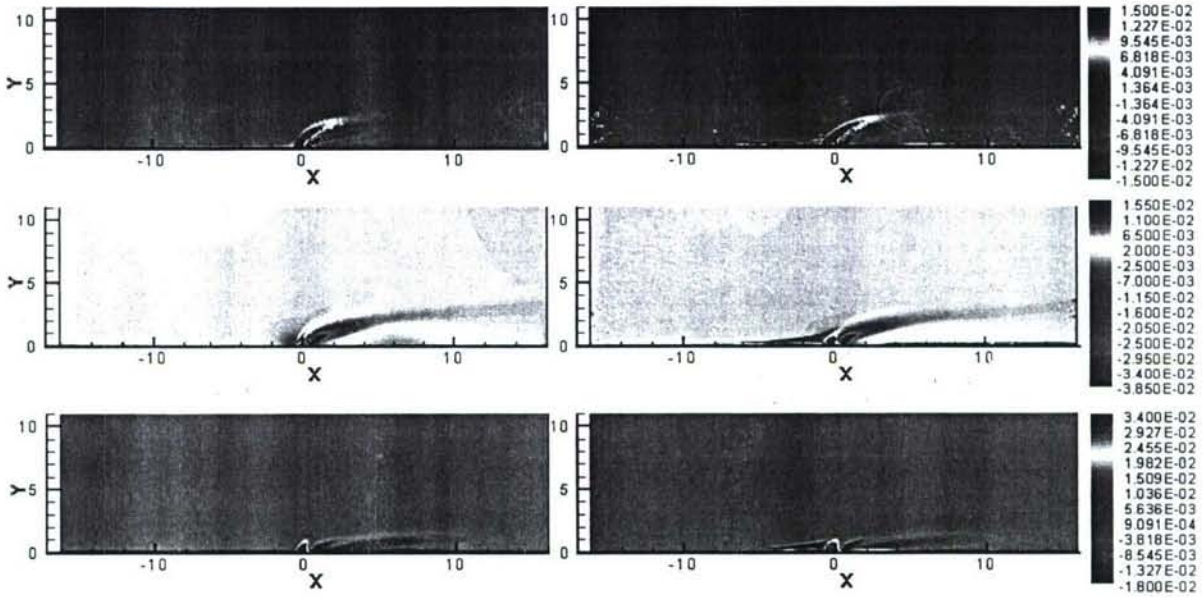

Figure 6 M=0.15, LDST/Cell Area, (Top Left)Structured Mesh Energy Source Term, (Top Right)Unstructured Mesh Energy Source Term, (Center Left)Structured Mesh X-Momentum Source Term, (Center Right)Unstructured Mesh X-Momentum Source Term, (Bottom Left)Structured Mesh Y-Momentum Source Term, (Bottom Right)Unstructured Mesh Y-Momentum Source Term

Equally important to demonstrating grid insensitivity is to show the flow variables obtained with the structured and unstructured grid unsteady solutions and to demonstrate that the LDST approach works for an unstructured grid. That is, show that one can take the LDSTs from the unstructured grid solution, insert them in a steady state solver as source terms and generate the time average solution; as was shown in the previous work for the structured grid. This is demonstrated nicely in Figures 7 and 8 below for the structured and unstructured grid solutions, respectively. The unsteady solution is computed on the complete geometry, including the synthetic jet, and time averaged to produce the figures on the left. The time average solution is then used to create the LDSTs as shown in Figures 4 and 5 for both grids. These LDSTs were then inserted into the steady state solver as source terms but without the details of the synthetic jet geometry to produce the time average solutions shown on the right in the figures. Again it is clear that there are minor differences between the structured and unstructured results but the LDST approach is clearly demonstrated for both grids. The next step is to explore the application of the NN-LDST approach built from time averaged solutions of this type.

The results obtained from using the original NN-LDST[18] in a steady state solver are shown next to recall its accuracy. Figure 9 shows the momentum thickness 10 mm downstream of the jet orifice plotted versus freestream Mach number and demonstrates nicely the ability of the original approach to follow time average solution trends. This same parameter will be used to define the quality of the modified approach when it is applied to different grids.

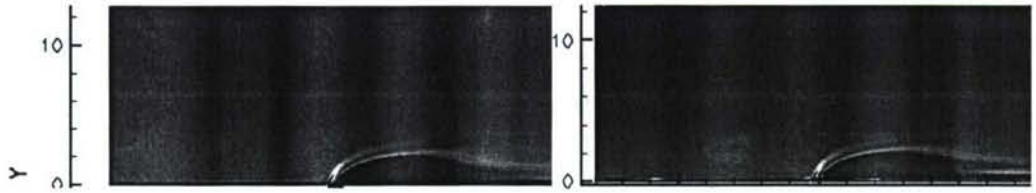

Figure 7 (Left) Structured Grid Vorticity Contours: Time Average of Unsteady Computations, (Right)Steady with LDSTs added

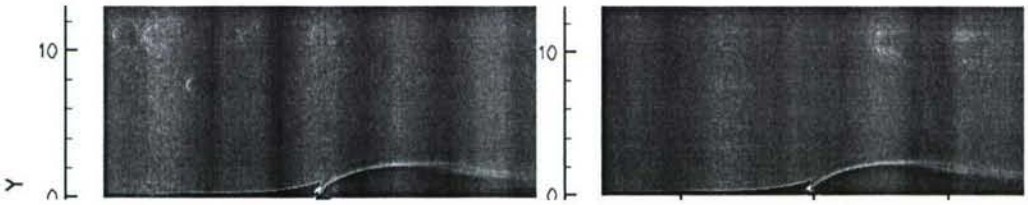

Figure 8 (Left) Unstructured Grid Vorticity Contours: Time Average of Unsteady Computations, (Right)Steady with LDSTs added

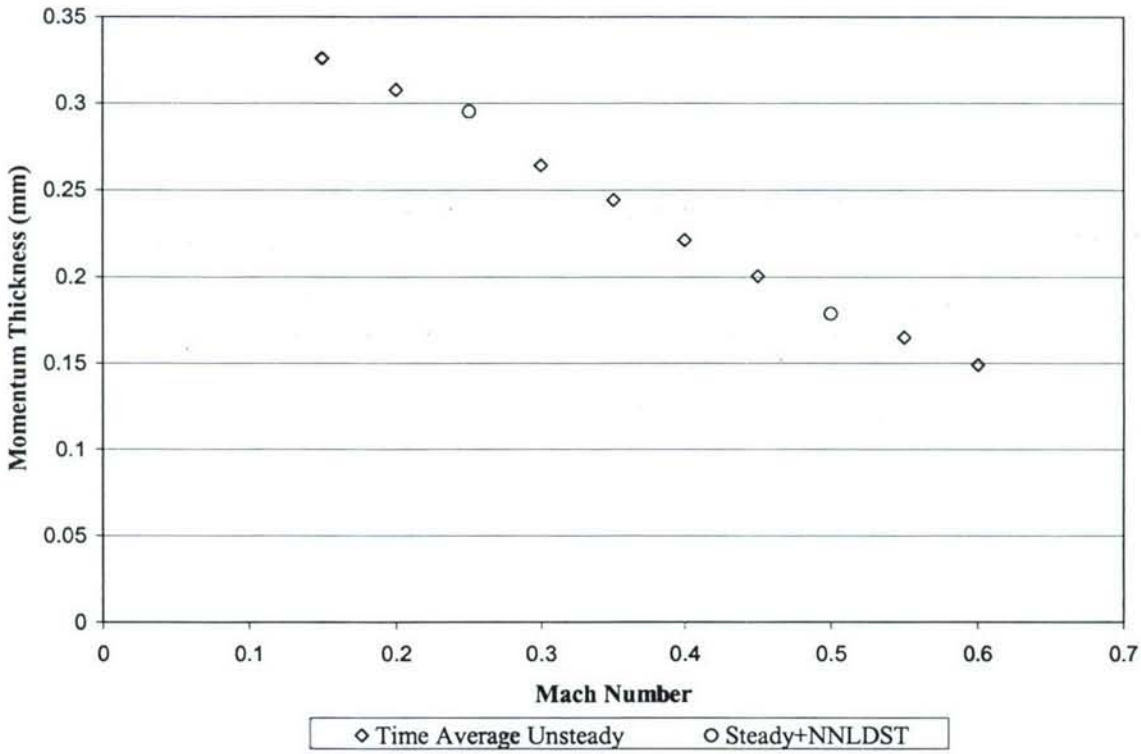

Figure 9 Momentum Thickness Computed 10mm Downstream of Orifice

Coarsened Grid Study

A modification of the original NN-LDST approach is now developed that allows the approach to be applied directly without additional training. The original approach produces the source terms on a cell by cell basis for a specific grid when cell center values are input. However, the LDSTs are not identical in this form when applied on different girds as shown by Figures 4 and 6. The modification to general grids then requires that the cell center of the new grid cell be used as input to the neural network, but again this gives the LDST for the original grid. Examples of this are shown in Figures 10, 12 and 14, and provide a false sense of security since they match each other nicely. However, the experience of Figures 4, 5 and 6 indicates that the pure LDST should be different on different grids, only the LDST on a cell volume basis should be identical. Clearly these results are not yet appropriate as they are only the original grid LDSTs depicted on the new grids. To obtain the appropriate LDSTs for the different grids a search routine is then needed to identify the cell on the original grid that contains the cell center location from the new grid. Once this cell is identified the original NN-LDST can be placed on the per cell area basis. The LDST per cell area can then be multiplied by the cell area from the new grid to create the LDST appropriate for the new grid. In the end the original NN-LDST module is applied without any additional neural network training.

The LDSTs per cell area were obtained by applying the above approach. Figures 10 through 15 show the LDSTs on several coarsened grids in which Δx is held constant throughout the domain with values of 0.1, 0.25 and 0.5. The original grid held a constant Δx=0.025 in the vicinity of the orifice but stretched Δx farther away. In all cases the y distribution remains the same. Figures 10, 12 and 14 show the source terms predicted on the new grids cell centers while figures 11, 13, and 15 depict the source terms on the coarsened grids after the cell transformation. Figures 11, 13 and 15 show that, as expected, the LDST predictions grow worse

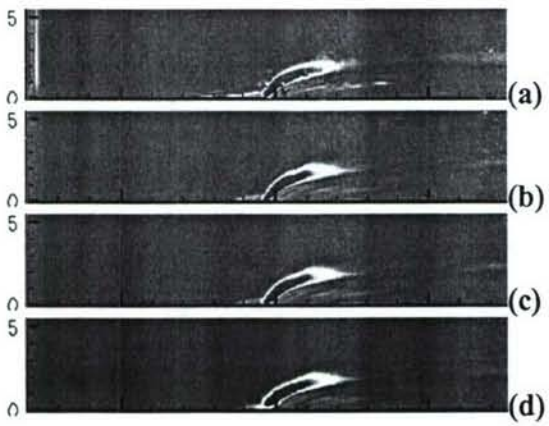

Figure 10 Energy Source Term: (a) Original Grid (b) Δx=0.1 (c) Δx=0.25 (d) Δx=0.5

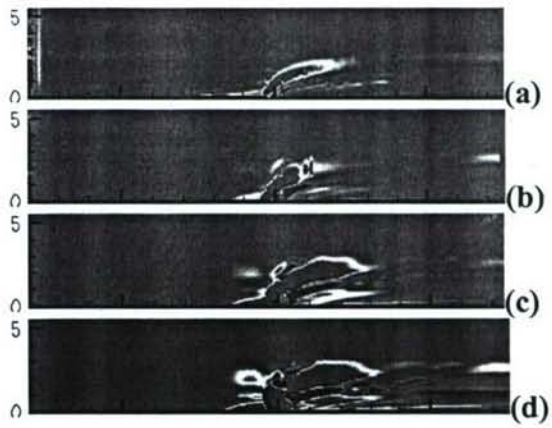

Figure 11 Energy Source Term utilizing Cell Area Approach: (a) Original Grid (b) Δx=0.1 (c) Δx=0.25

as the grid is coarsened. It should be kept in mind that the grid with Δx=0.5 is nearly 20 times coarser than the original grid. A steady state solver was then used with the LDSTs as source terms, as depicted in Figures 11, 13 and 15, in order to obtain the time average solution without modeling the synthetic jet geometry. The quality of the approach can be seen from Figure 16, where the momentum thickness 10 mm downstream of the synthetic jet orifice is plotted for

several coarsened grids for a Mach number of 0.3. The solid line represents the momentum thickness from the time average of the unsteady solution. Clearly, the momentum thickness is predicted poorly as the grid becomes coarser, but the prediction on the finest grid, with roughly 4 times the grid spacing, is quite good.

The results demonstrate that the modified NN-LDST technique can be used on coarsened grids but that its quality will degrade with grid resolution. Future efforts will be directed at improving this approach and will focus on training the neural network using LDSTs on a per cell area basis, including cell area directly as a parameter in the NN-LDST output and/or using the original NN-LDST in such a way that the LDSTs are summed over the new grid cell area rather than mapped. However, the overall result is very encouraging.

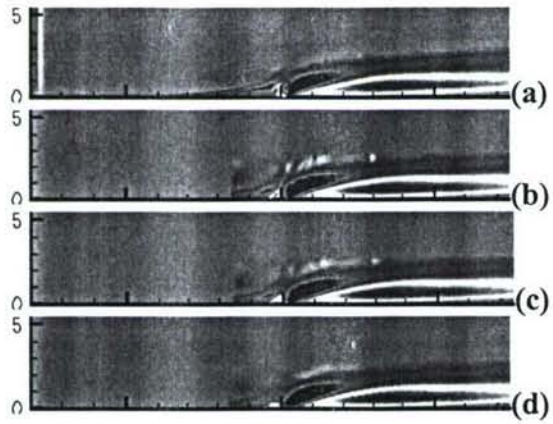

Figure 12 X-Momentum Source Terms: (a) Original Grid (b) Δx=0.1 (c) Δx=0.25 (d) Δx=0.5

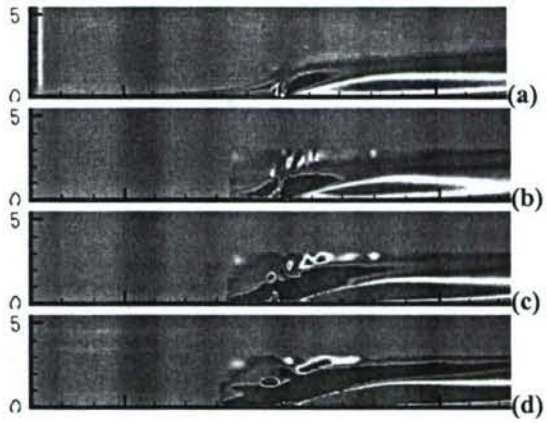

Figure 13 X-Momentum Source Term using Cell Area Approach: (a) Original Grid (b) Δx=0.1 (c) Δx=0.25 (d) Δx=0.5

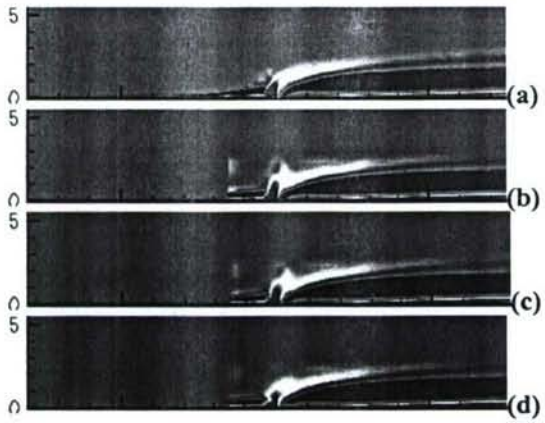

Figure 14 Y-Momentum Source Terms: (a) Original Grid (b) Δx=0.1 (c) Δx=0.25 (d) Δx=0.5

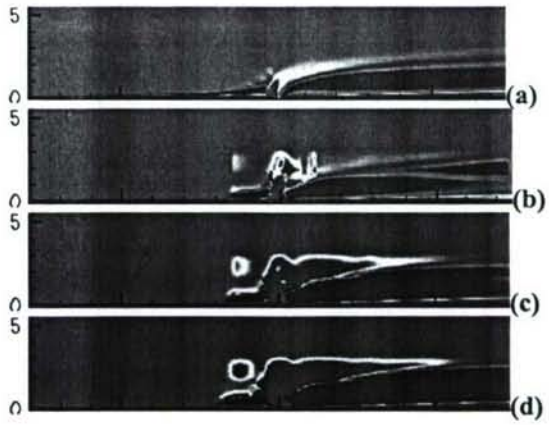

Figure 15 Y-Momentum Source Term using Cell Area Approach: (a) Original Grid (b) Δx=0.1 (c) Δx=0.25 (d) Δx=0.5

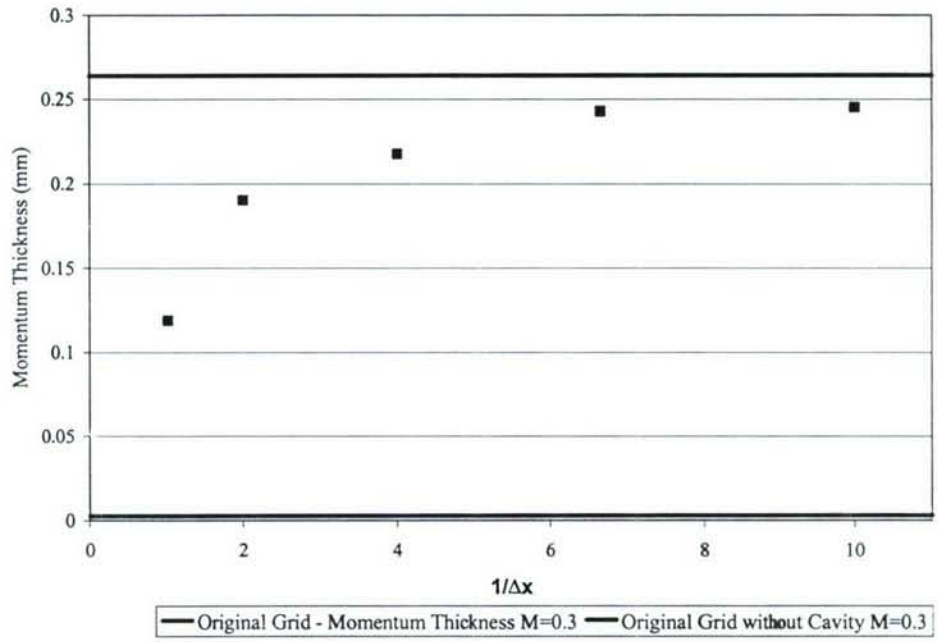

Figure 16 Momentum Thickness for Coarsened Grids 10mm Downstream of Orifice

Conclusions

The NN-LDST approached developed previously has been shown to have limited grid sensitivity. In particular:

- LDSTs obtained from the time average of unsteady solution computed on structured and unstructured meshes can be used as source terms in a steady solver to reproduce the time average solution.
- Pure LDST results cannot be directly compared for different grids as they must be placed on a per cell area basis to be considered universal.
- The NN-LDST approach developed on a single grid can be applied to other more general grids by developing an appropriate cell area transformation and utilizing their per cell area form.

Acknowledgement/Disclaimer

This work was sponsored (in part) by the Air Force Office of Scientific Research, USAF, under grant F49620-02-0-0092. The views and conclusions contained herein are those of the author and should not be interpreted as necessarily representing the official policies or endorsements, either expressed or implied, of the Air Force Office of Scientific Research or the U.S. Government.

References

1. Seifert, A., Bachar, T, Koss, D., Shepshelovich, M. and Wygnanski, I., "Oscillatory Blowing: A Tool to Delay Boundary-Layer Separation," *AIAA Journal*, Vol. 31, No 11, November 1993.
2. Seifert, A., Darabi, A. and Wygnanski, I., "Delay of Airfoil by Periodic Excitation," *Journal of Aircraft*, Vol. 33, No 4, 1996.
3. Smith, B.L. and Glezer, A., "Vectoring and Small Scale Motions Effected in Free Shear Flows Using Synthetic Jet Actuators," AIAA-97-0213, 35th Aerospace Sciences Meeting and Exhibit, Reno, NV, 1997.
4. Rediniotis, O. K., Ko, J., Yue, X., "Synthetic Jets, Their Reduced Order Modeling and Applications to Flow Control", AIAA Paper 99-1000, 1999.
5. Kral L. D.: "Active Flow Control Technology", ASME Fluids Engineering Division Technical Brief.
6. Amitay, M., Smith, D.R., Kibens, V., Parekh, D.E., Glezer, A., "Aerodynamic Flow Control over an Unconventional Airfoil Using Synthetic Jet Actuators", *AIAA Journal*, Vol. 39, No. 3, March 2001.
7. Amitay, M., Kibens, V., Parekh, D., and Glezer, A., "The Dynamics of Flow Reattachment over a Thick Airfoil Controlled by Synthetic Jet Actuators", AIAA Paper 99-1001, 1999.
8. Hassan, A. A., and Munts, E. A., "Transverse and Near-Tangent Synthetic Jets for Aerodynamic Flow Control", AIAA Paper 200-4334, 2000.
9. Mittal, R., Rampunggoon, P., Udaykumar, H. S., "Interaction of a Synthetic Jet with a Flat Plate Boundary Layer", AIAA Paper 2001-2773, 2001.
10. McCormick, D.C., "Boundary Layer Separation Control with Directed Synthetic Jets", AIAA Paper 2000-0529, 2000.
11. Ritchie, B., Seitzmann, J., "Mixing Control of Fuel Jets Using Synthetic Jet Technology: Scalar Field Measurements", AIAA Paper 99-0448, 37th Aerospace Sciences Meeting and Exhibit, Reno, NV, 1999.
12. Chen, Y., Liang, S., Aung, K., Glezer, A., Jagoda, J., "Enhanced Mixing in a Simulated Combustor Using Synthetic Jet Actuators", AIAA Paper 99-0449, 37th Aerospace Sciences Meeting and Exhibit, Reno, NV, 1999.
13. Wang, H., Menon, S., "Fuel-Air Mixing Enhancement by Synthetic Microjets", *AIAA Journal*, Vol. 39, No. 12, December 2001.
14. Camci, C., Herr, F., "Forced Convection Heat Transfer Enhancement Using a Self-oscillating Impinging Planar Jet".
15. Lukovic, B., Gangwar, A., and Orkwis, P.: "Modeling unsteadiness in steady cavity simulations. II - Neural network modeling", AIAA Paper 2001-154, 39th AIAA Aerospace Sciences Meeting and Exhibit, Reno, NV 2001.

16. Lukovic, B., Orkwis, P., Turner, M. and Sekar B., "Effect of Cavity *L/D* Variations on Neural Network-Based Deterministic Unsteadiness Source Terms", AIAA Paper 2002-0857, 2002.

17. Lukovic, B., Orkwis, P. and Turner, M., "Modeling Unsteady Cavity Flows With Translating Walls", AIAA Paper 2002-3288, 2002.

18. Pes, M., Lukovic, B., Orkwis, P., Turner, M., "Modeling of Two Dimensional Synthetic Jet Unsteadiness Using Neural Network-Based Deterministic Source Terms," AIAA Paper 2002-2860, 32nd AIAA Fluid Dynamics Conference and Exhibit, St. Louis, MS, 2002.

19. Lee, D., Orkwis, P., Turner, M., Filz, C., Pes, M., Caldwell, N., "Numerical Analysis of Two Dimensional Synthetic Jets in Cross Flow at Low Mach Number", AIAA Paper 2003-0637, 41st AIAA Aerospace Sciences Meeting and Exhibit, Reno, NV, 2003.

20. Filz, C., Lee, D., Orkwis, P., Turner, M., "Modeling of Two Dimensional Directed Synthetic Jets Using Neural Network-Based Deterministic Source Terms", AIAA Paper 2003-3456, 33rd AIAA Fluid Dynamics Conference and Exhibit, Orlando, FL, 2003.

21. Levenberg, K., "A Method for the Solution of Certain Non-linear Problems in Least Squares", *Quarterly Applied Mathematics*, Vol. 2, 1944, pp. 164-168.

22. Marquardt, D. W., "An Algorithm for Least Squares Estimation of Nonlinear Parameters", *Journal of Society of Industrial Applied Mathematics*, Vol. 11, No.2, 1963, pp. 431-441.

23. Cybenko, G., "Approximations by Superpositions of Sigmoidal Functions", *Mathmatics of Control, Signals, and Systems*, No.2, 1989, pp. 303-314.

24. Hornik, K., "Multilayer Feedforward Networks are Universal Approximators", *Neural Networks*, No.2, 1989, pp. 359-366.

25. White, H., "Connectionist Nonparametric Regression: Multilayer Feedforward Networks can Learn Arbitrary Mappings", *Neural Networks*, No.3, 1990, pp. 535-549.

26. Osher, S., and Chakravarthy, S. R., "Very High Order Accurate TVD Schemes", In *Oscillation Theory, Computation, and Methods of Compensated Compactness, The IMA Volumes in Mathematics and Its Applications,* Volume 2, eds. C. Dafermos, J. L. Erikson, D. Kinderleher, and M. Slemrod, pp. 229-271, New York: Springer-Verlag, 1986.

27. Goldberg, U., Peroomian, O., Chakravarthy, S., "A Wall-Distance-Free k-ϵ Model With Enhanced Near-Wall Treatment", *Journal of Fluids Engineering*, Vol. 120, pp. 457-462, 1998.

Personnel Supported During Duration of Grant

Terry Daviaux	Graduate Student, University of Cincinnati
Paul D. Orkwis	Associate Professor, University of Cincinnati

Publications

1. Daviaux, T., and Orkwis, P.D., "On the Grid Insensitivity of an Advanced Neural Network Based Model for Synthetic Jet Flow Fields," AIAA Paper 2006-0321, 44th AIAA Aerospace Sciences Meeting, Reno, NV, January 2006.

Honors & Awards Received

AFRL Point of Contact

Carl Tilmann, AFRL/VAAA, WPAFB, OH, Phone 937-255-4077.

- Met with him at AIAA Aerospace Sciences Meeting in Reno, NV, January 2005.
- Met with him at the AIAA Dayton-Cincinnati Section Aerospace Sciences Symposium, March 2005.
- Met at Wright-Patterson AFB, May 2005